Prestress and Area Compressibility of Actin Cortices Determine the Viscoelastic Response of Living Cells

Andrea Cordes,[1] Hannes Witt,[2] Aina Gallemí-Pérez,[2] Bastian Brückner,[1] Florian Grimm,[1,3] Marian Vache,[1] Tabea Oswald,[4] Jonathan Bodenschatz,[1] Daniel Flormann,[5] Franziska Lautenschläger,[5,6] Marco Tarantola,[2,*] and Andreas Janshoff[1,†]

[1]*Institute of Physical Chemistry, Georg-August-Universität Göttingen, 37077 Göttingen, Germany*
[2]*Max Planck Institute for Dynamics and Self-Organization, 37077 Göttingen, Germany*
[3]*Abberior GmbH, 37077 Göttingen, Germany*
[4]*Institute of Org. and Biomolecular Chemistry, Georg-August-Universität Göttingen, 37077 Göttingen, Germany*
[5]*Leibniz Institute for New Materials, 66123 Saarbrücken, Germany*
[6]*NT faculty, Experimental Physics, Saarland University, 66123 Saarbrücken, Germany*

(Received 24 September 2019; accepted 15 July 2020; published 6 August 2020)

Shape, dynamics, and viscoelastic properties of eukaryotic cells are primarily governed by a thin, reversibly cross-linked actomyosin cortex located directly beneath the plasma membrane. We obtain time-dependent rheological responses of fibroblasts and MDCK II cells from deformation-relaxation curves using an atomic force microscope to access the dependence of cortex fluidity on prestress. We introduce a viscoelastic model that treats the cell as a composite shell and assumes that relaxation of the cortex follows a power law giving access to cortical prestress, area-compressibility modulus, and the power law exponent (fluidity). Cortex fluidity is modulated by interfering with myosin activity. We find that the power law exponent of the cell cortex decreases with increasing intrinsic prestress and area-compressibility modulus, in accordance with previous finding for isolated actin networks subject to external stress. Extrapolation to zero tension returns the theoretically predicted power law exponent for transiently cross-linked polymer networks. In contrast to the widely used Hertzian mechanics, our model provides viscoelastic parameters independent of indenter geometry and compression velocity.

DOI: 10.1103/PhysRevLett.125.068101

Many cellular processes such as adhesion, motility, growth, and development are tightly associated with the mechanical properties of cells and their environment [1–3]. Vitality and fate of cells are often directly inferred from their elastic properties [4–6]. In search for effective and standardized mechanical phenotyping of living cells, several tools have been developed that permit precise and fast measurements [7]. The response of cells to external deformation is primarily attributed to the viscoelasticity of the cellular cortex [5,8–10]. The cortex forms a composite shell consisting of a compliant but contractile actin mesh with a large number of actin-binding proteins coupled to the plasma membrane [11,12]. The thin actin cortex can be contracted by the action of motor proteins such as myosin II, resulting in a measurable prestress that provides resistance against deformation at low strain [10,13]. It was found that rheological parameters of compliant cells such as the complex shear modulus generally obey a power law dependency $G^* \propto \omega^\beta$ over multiple decades in frequency ω [14,15]. The dimensionless power law coefficient β characterizes the degree of fluidity and energy dissipation upon deformation, where $\beta = 0$ represents an ideal elastic solid and $\beta = 1$ a Newtonian liquid. Values obtained for the power law exponent of living cells usually range between 0.2–0.4 for adherent cells suggesting glassy dynamics [4,14]. *In vitro* experiments and theory suggest that transiently cross-linked actin networks generate a broad spectrum of relaxation times typical for a power law behavior with $\beta = 0.5$ below the characteristic frequency ($2\pi/\tau_{\text{off}}$, τ_{off} being the unbinding time of the cross-linker) [16]. It is still unclear why rheological properties found for living cells and those of artificial actin cortices are different. Recently, Mulla *et al.* could show that transient cross-linking of actin filaments combined with external stress leads to lowering of the power law exponent [17]. Here, the goal is to examine how internal stress changes the viscoelastic properties of living cells. Therefore, we require a viscoelastic model that permits to relate the prestress of cells to the fluidity obtained from deformation-relaxation experiments. Our viscoelastic model of the cortex is based on time-independent cortical prestress to capture the contractility of the actomyosin cortex and the power law rheology suitable to describe the time-dependent deformation and relaxation of confluent and weakly adherent cells. Drugs like blebbistatin [18] and calyculin *A* [19] were administrated to decrease or increase contractility. We found that cortex fluidity decreases with increasing prestress recovering a power law exponent of

 © 2020 American Physical Society

0.5 expected for transiently cross-linked actin networks in the absence of tension [20]. From scrutinizing the cortex thickness and its mesh size [Figs. 1(a)–1(d), [21]) with scanning electron microscopy and fluorescence microscopy, it is safe to treat the cortex as a two-dimensional continuous material neglecting bending stiffness and area shear modulus [42]. The cortex resists deformation only by its area compressibility modulus and prestress. The prestress term T_0 mirrors predominately actin architecture and myosin activity of the cortex as shown by Paluch and coworkers [10,11] but also includes contributions from membrane tension that occur due to attachment of the actin network to the plasma membrane via specialized cross-liners such as ezrin or moesin [13,22,43]. The area compressibility modulus K_A is the 2D elastic modulus of the shell and reflects its time-dependent elastic resistance of the active shell to area increase [23]. We refer to this model as the viscoelastic Evans model throughout the text due to his seminal and initial work on cortex mechanics [42]. Viscoelasticity of the 2D area compressibility modulus is assumed to follow a power law. Minimizing free energy assuming constant volume leads to minimal surfaces of constant curvature. The force (f) balance at the equatorial radius for cells between two parallel plates reads:

$$f = \frac{2\pi R_0 R_i^2}{R_0^2 - R_i^2}(T_0 + K_A\alpha) \tag{1}$$

with R_0 as the equatorial radius, R_i the contact radius, $\alpha = (\Delta A/A_0)$ the areal strain, T_0 the prestress, and K_A the area-compressibility modulus of the cortex. It is straightforward to cast the model into a nondimensional form that permits us to write Eq. (1) as $g(\xi) = (f/R_cT)$, with $\xi = z_p/R_c$. z_p is the distance between the plates, R_c the initial radius of the cell in suspension and T denotes the overall homogeneous tension. Hence, $g(\xi)$ and $\alpha(\xi)$ are generic functions that only need to be computed once. Both functions can easily be approximated by polynomials $g(\xi) \approx \sum_{i=1}^{3} c_i\xi^i$ and $\alpha(\xi) \approx \sum_{i=1}^{3} d_i\xi^i$ permitting one to obtain an analytical solution of the corresponding elastic-viscoelastic problem [21]. The general hereditary integral for the restoring force during parallel-plate compression [$0 < t < t_m$, Eq. (2)] and relaxation ($t > t_m$) reads [24]:

$$f = g(\xi)R_c\left(T_0 + \int_0^s \tilde{K}_A(t-\tau)\frac{\partial\alpha(\tau)}{\partial\tau}d\tau\right) \tag{2}$$

with $s = t$ for compression and $s = t_m$ for relaxation ($\dot{\alpha} = 0$). The integrals can be solved by using $\xi \approx (v_0t/R_c)$ for compression with the constant velocity v_0 and assuming a power law behavior of $\tilde{K}_A = K_A(t/t_0)^{-\beta}$ with the time-scaling parameter t_0 [21]. The general scheme described here can also be used to describe the deformation of adherent and confluent cells with various indenter geometries [21].

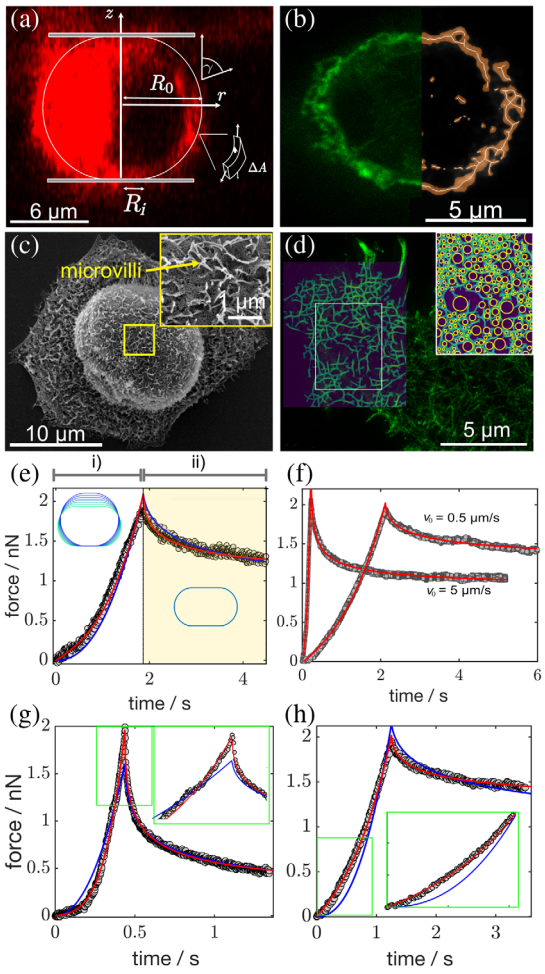

FIG. 1. (a) CLSM image (xz plane) of a MDCK II cell (plasma membrane stained with CellMask) clamped between cantilever and substrate. White lines show the parametrization. (b) Left side: STED image (xy plane) of the cellular cortex (green: actin) of a MDCK II cell. Right side: reconstruction of the cortex [21]. (c) SEM image of a MDCK II cell revealing its cortex structure (right). (d) Mesh size analysis of cortex extracts [21]. (e) Typical compression (i) at $v_0 = 0.5$ μm/s followed by force relaxation (ii) of a MDCK II cell and fits according to the Hertz model (blue line, $E_0 = 450$ Pa, $\beta = 0.22$) and the Evans model (red line, $T_0 = 0.75$ mN/m, $K_A = 0.44$ N/m, $\beta = 0.49$). The inset shows the time evolution of the contour. (f) Varying the compression velocity does not impact the fitting results: $T_0 = 0.83$ mN/m, $K_A = 0.39$ N/m, $\beta = 0.42$ for a MDCK II cell compressed with 0.5 μm/s and $T_0 = 0.57$ mN/m, $K_A = 0.24$ N/m, $\beta = 0.43$ for the same cell compressed at 5 μm/s. (g) Compression-relaxation curve of a MDCK II cell after blebbistatin treatment showing substantial softening ($v_0 = 0.5$ μm/s). Blue line: Hertz fit ($E_0 = 62$ Pa, $\beta = 0.41$). Red line: Evans fit ($T_0 = 0.02$ mN/m, $K_A = 0.002$ N/m, $\beta = 0.57$). (h) MDCK II cell after calyculin A treatment. Blue line: Hertz fit ($E_0 = 1097$ Pa, $\beta = 0.18$). Red line: Evans fit ($T_0 = 1.6$ mN/m, $K_A = 2.36$ N/m, $\beta = 0.4$).

We used an atomic force microscope to examine the viscoelastic properties of fibroblasts (3T3) and MDCK II

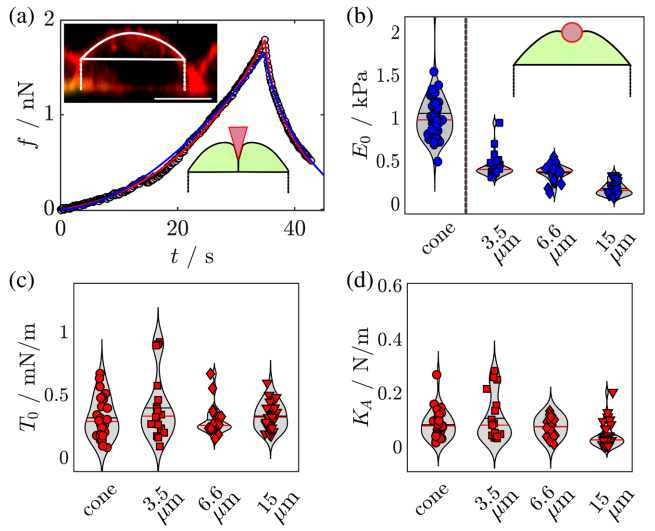

FIG. 2. (a) Indentation-retraction curve of a confluent MDCK II cell probed with a conical indenter and subject to fitting with the viscoelastic Evans model (red line) and Hertz model (blue line), respectively. The insets show a cross section of the cell and the computed shape after indentation, respectively (scale bar: 10 μm). (b) Young's modulus E_0 of confluent MDCK II cells obtained for different indenter geometries (cone, spheres with various diameters). (c),(d) Corresponding T_0 and K_A obtained from fitting with the viscoelastic Evans model.

cells in a confluent and weakly adhered state. For parallel-plate compression experiments, tipless cantilevers were used to compress weakly adhering cells (Fig. 1), while cantilevers equipped with spherical (diameter: 3.5, 6.6, 15 μm) and conical tips ($\approx$18° half cone angle) were employed for indentation experiments (Fig. 2). We used constant approach and retraction velocities between 0.5–25 μm/s and a relaxation time of several seconds. As indicated, either cytochalasin D, blebbistatin or calyculin A were added to cell medium shortly before cell seeding [21].

Figure 1(e) shows a typical compression-relaxation experiment of a single MDCK II cell using parallel-plate geometry. It is divided into the compression phase (i) during which the cell is loaded at constant velocity until the yield force is reached at t_m and subsequent force relaxation (ii) at constant distance between the plates. The full curve from the contact to the end of the relaxation curve was modeled with Eq. (2) (red line) by adapting the three fitting parameters, cortical tension T_0, area-compressibility modulus K_A, and the power law exponent β. Equation (2) requires input regarding the size of each cell (R_c), which was measured using light microscopy prior to compression. For comparison, we also fitted the viscoelastic Hertz model (blue lines) to the data, which falls short in describing the curves, especially at low strain where the prestress T_0 dominates, and directly at the onset of relaxation [21]. The prestress captures the linear onset of the indentation or compression curve since at low strain the force response can be approximated as $f \approx T_0 c_1 z_p$, with c_1 the leading coefficient of the polynomial $g(\xi)$ at small z_p. This can be illustrated by attempting to fit force-indentation curves with the Evans model using $T_0 = 0$ [21]. As a consequence, β values obtained from viscoelastic Hertz mechanics are systematically smaller than those provided by the Evans model [21]. Figure 1(f) shows representative fits of Eq. (2) to compression-relaxation curves of MDCK II cells loaded with 0.5 and 5 μm/s, respectively. As required, the viscoelastic parameters are not impacted in this moderate velocity regime. However, since hydrodynamic drag at the onset of the compression curve is only negligible at low approach speed, subsequent experiments were carried out predominately at low speed ($\leq$1 μm/s). The impact of blebbistatin and calyculin A on the compression-relaxation curves is shown exemplarily in Figs. 1(g) and 1(h), while mean values are provided in Fig. 3. The softening of cells due to stalling of myosin motors is mirrored in smaller cortical tension and larger power law exponents, compared to untreated cells. This is particularly distinct for MDCK II cells, while fibroblasts in suspension are less affected [21]. An increase in β is indicative of cortex fluidization, which we attribute to a loss of transient cross-links otherwise provided by myosin bundles. Administration of calyculin A, which is a phosphatase inhibitor that increases myosin II processivity, generates only slightly larger prestress (contractility) and smaller β values, indicative of cell stiffening. Knowledge of cortex thickness and mesh size [[21], Figs. 1(b) and 1(d)] allows us to estimate the area compressibility modulus from $K_A \approx (3k_BTl_p^2/\zeta^2)(d/l_c^3)$, with the distance between cross-links $l_c \approx \zeta^{4/5} l_p^{1/5}$ and the persistence length l_p of 17 μm [20]. With a mesh size ζ of 25–250 nm and a cortex thickness d in the range of 100–1500 nm [Figs. 1(b) and 1(d), [21]] we arrive for K_A at values ranging from 0.3 mN/m up to >10 N/m, which is in good accordance with our results. Notably, the same arguments leave us with Young's modules in the range of 3 up to 7 MPa, which is at least two orders of magnitude higher than values obtained from the Hertz model [Fig. 2(b)]. Experimentally, the validity of a viscoelastic model can be verified by testing whether the two models generate viscoelastic parameters that are independent of the choice of indenter geometry or size. For this purpose, we used confluent MDCK II cells, which are easily probed with different indenter geometries and adapted the model according to the new overall geometry (Fig. 2, [21]). Generally, confluent MDCK II cells are softer and more fluid compared to weakly adhered cells. Importantly, we find that the Young's modulus obtained from the Hertz model depends on the size of the indenter. Larger radii of spherical and conical indenters result in systematically smaller Young's modules rendering the Hertz model unsuitable to provide geometry-invariant viscoelastic parameters. In contrast, neither cortex tension nor area compressibility modules depend on the indenter size. It is,

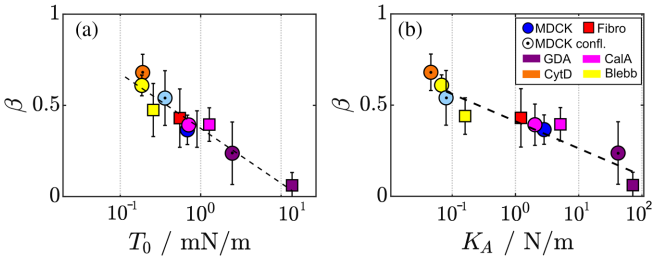

FIG. 3. Power law exponents β of MDCK II cells (circles) and fibroblasts (squares) as a function of prestress T_0 and area-compressibility modulus K_A subject to different indenter geometries and drug treatments (see legend). MDCK confl.: confluent MDCK II cells deformed with conical and spherical indenters (light blue, data compiled from Fig. 2); Blebb: Blebbistatin; CytD: Cytochalasin D; CalA: Calyculin A; GDA: Glutardialdehyde; Dashed lines are fits illustrating the logarithmic dependencies [15].

however, conceivable that other cell types are sufficiently well described by contact models. The Evans model is suitable to describe force relaxation curves over the entire experimental timescale independent of compression speed and indenter geometry. A poroelastic behavior of the cells (MDCK II) was proposed to describe the initial relaxation response after fast loading [44]. Here, we show that this initial drop is well captured by simple power law rheology but requires treatment of the actomyosin cortex as a prestressed shell [Fig. 1(g)].

Therefore, the Evans model paves the way to address a fundamental problem in cell rheology, the apparent discrepancy between the rheology of living cells with glassy dynamics providing β values of 0.2 and the rheology of transiently cross-linked actin networks expecting β values of 0.5 reflecting the broad distribution of relaxation times [16]. First, we found that the power law exponents obtained from the Hertz model are systematically lower ($\bar{\beta} = 0.2$) than those from the Evans model ($\bar{\beta} = 0.4$). Second, cells with stiffer cortices display a smaller power law exponent (Fig. 3). Specifically, β decreases for both cell types and all treatments logarithmically with K_A [Fig. 3(b), [21]]. This behavior has also been predicted by Gardel *et al.* [45] for the differential modulus and Kollmannsberger *et al.* [15] for the compliance of various cell types. Importantly, the model also allows to correlate internal prestress with fluidity, which suggests that the viscoelastic parameters are not independent. By compiling all data (cell types, indenter geometries, and drug treatment), we found that an increase in T_0 is accompanied by a reduction of the power law coefficient [Fig. 3(a)], which suggests that cells with a more contractile cortex are also less fluid. We also artificially increased tension by addition of glutardialdehyde (GDA) that contracts the cortex to generate solidlike shells with extremely low β values. Vice versa, cytochalasin D, a potent inhibitor of actin polymerization softens the cells and increases fluidity to a similar extent than blebbistatin (Fig. 3). Recently, Mulla *et al.* found that artificial actin networks show a decrease of β with increasing stress [17], suggesting that the glassy dynamics of the cortex are a natural consequence of transient cross-links combined with intrinsic prestress. Here, we can confirm that increased myosin activity increases the prestress and in turn also lowers the power law exponent. In the absence of motor activity and therefore low prestress T_0, β is close to 0.5, as expected for reversibly cross-linked actin filaments at low frequency [16]. Notably, Yao *et al.* examined the rheology of actin networks, cross-linked by α actinin, showing that external stress delays the onset of relaxation and flow, essentially extending the regime of solidlike behavior to much lower frequencies [46]. Taken together, the cortex forms an active shell, mechanically characterized by prestress, area compressibility and fluidity. At low strain the prestress or effective surface tension [23] dominates and reflects actin architecture (filament length, mesh size, and thickness), attachment to the plasma membrane, and contractility [10,43]. At larger strain, area dilatation of the shell becomes appreciable [22,47] and the response to compression becomes time dependent.

In conclusion, we found that a viscoelastic shell model is capable of describing cell compression and relaxation experiments over the entire timescale in a consistent manner. MDCK II cells show a decrease in cortex fluidity with increasing prestress and area compressibility modulus, thereby closing the gap between rheological experiments of artificial actin networks and living cells.

The work was financially supported by the DFG [Grant No. SFB937(A8): A. J. and M. T.; Grant No. SFB 1027(A9): F. L.) and the VW foundation ("Living Foams": A. J. and M. T.).

*mtarant@gwdg.de
†ajansho@gwdg.de

[1] B. G. Godard and C.-P. Heisenberg, Curr. Opin. Cell Biol. **60**, 114 (2019).
[2] J. R. Lange and B. Fabry, Exp. Cell Res. **319**, 2418 (2013).
[3] D. A. Fletcher and R. D. Mullins, Nature (London) **463**, 485 (2010).
[4] J. Rother, H. Nöding, I. Mey, and A. Janshoff, Open Biol. **4**, 140046 (2014).
[5] J. R. Staunton, B. L. Doss, S. Lindsay, and R. Ros, Sci. Rep. **6**, 19686 (2016).
[6] P. D. Garcia and R. Garcia, Nanoscale **10**, 19799 (2018).
[7] P.-H. Wu *et al.*, Nat. Methods **15**, 491 (2018).
[8] M. Kelkar, P. Bohec, and G. Charras, Curr. Opin. Cell Biol. **66**, 69 (2020).
[9] T. M. Svitkina, Trends Cell Biol. **30**, 556 (2020).
[10] P. Chugh, A. G. Clark, M. B. Smith, D. A. D. Cassani, K. Dierkes, A. Ragab, P. P. Roux, G. Charras, G. Salbreux, and E. K. Paluch, Nat. Cell Biol. **19**, 689 (2017).
[11] P. Chugh and E. K. Paluch, J. Cell Sci. **131**, jcs186254 (2018).

[12] R. G. Fehon, A. I. McClatchey, and A. Bretscher, Nat. Rev. Mol. Cell Biol. **11**, 276 (2010).
[13] G. Salbreux, G. Charras, and E. Paluch, Trends Cell Biol. **22**, 536 (2012).
[14] B. Fabry, G. N. Maksym, J. P. Butler, M. Glogauer, D. Navajas, and J. J. Fredberg, Phys. Rev. Lett. **87**, 148102 (2001).
[15] P. Kollmannsberger and B. Fabry, Annu. Rev. Mater. Res. **41**, 75 (2011).
[16] C. P. Broedersz, M. Depken, N. Y. Yao, M. R. Pollak, D. A. Weitz, and F. C. MacKintosh, Phys. Rev. Lett. **105**, 238101 (2010).
[17] Y. Mulla, F. C. MacKintosh, and G. H. Koenderink, Phys. Rev. Lett. **122**, 218102 (2019).
[18] K. A. Beningo, K. Hamao, M. Dembo, Y. li Wang, and H. Hosoya, Arch. Biochem. Biophys. **456**, 224 (2006).
[19] L. Chartier, L. L. Rankin, R. E. Allen, Y. Kato, N. Fusetani, H. Karaki, S. Watabe, and D. J. Hartshorne, Cell Motil. Cytoskeleton **18**, 26 (1991).
[20] M. L. Gardel, Science **304**, 1301 (2004).
[21] See the Supplemental Material at http://link.aps.org/supplemental/10.1103/PhysRevLett.125.068101 for for details, which includes Refs. [10,15,20,22–41].
[22] A. Pietuch, B. R. Brückner, T. Fine, I. Mey, and A. Janshoff, Soft Matter **9**, 11490 (2013).
[23] E. Fischer-Friedrich, Y. Toyoda, C. J. Cattin, D. J. Müller, A. A. Hyman, and F. Jülicher, Biophys. J. **111**, 589 (2016).
[24] R. Christensen, *Theory of Viscoelasticity* (Elsevier, New York, 1982).
[25] T. M. Svitkina, A. B. Verkhovsky, and G. G. Borisy, J. Struct. Biol. **115**, 290 (1995).
[26] H. Nöding, M. Schön, C. Reinermann, N. Dörrer, A. Kürschner, B. Geil, I. Mey, C. Heussinger, A. Janshoff, and C. Steinem, J. Phys. Chem. B **122**, 4537 (2018).
[27] K. Bando, J. Biomech. Eng. **136**, 101003 (2014).
[28] M. Biro, Y. Romeo, S. Kroschwald, M. Bovellan, A. Boden, J. Tcherkezian, P. P. Roux, G. Charras, and E. K. Paluch, Cytoskeleton **70**, 741 (2013).
[29] C. Delaunay, J. Math. Pures Appl. **6**, 309 (1841).
[30] A. Dzementsei, D. Schneider, A. Janshoff, and T. Pieler, Biol. Open **2**, 1279 (2013).
[31] T. M. Svitkina, Int. J. Biochem. Cell Biol. **86**, 37 (2017).
[32] J. L. Hutter and J. Bechhoefer, Rev. Sci. Instrum. **64**, 1868 (1993).
[33] D. Flormann, M. Schu, E. Terriac, M. Koch, S. Paschke, and F. Lautenschläger, bioRxiv (2020) https://doi.org/10.1101/2020.01.06.896761.
[34] S. Münster and B. Fabry, Biophys. J. **104**, 2774 (2013).
[35] H. Elmoazzen, J. Elliott, and L. McGann, Cryobiology **45**, 68 (2002).
[36] K. Schulze, S. Zehnder, J. Urueña, T. Bhattacharjee, W. Sawyer, and T. Angelini, J. Biomech. **53**, 210 (2017).
[37] B. R. Brückner, H. Nöding, and A. Janshoff, Biophys. J. **112**, 724 (2017).
[38] R. Dimova and C. Marques, *The Giant Vesicle Book* (CRC Press, Taylor & Francis Group, Boca Raton, 2019).
[39] G. T. Charras, C.-K. Hu, M. Coughlin, and T. J. Mitchison, J. Cell Biol. **175**, 477 (2006).
[40] A. R. Harris and G. T. Charras, Nanotechnology **22**, 345102 (2011).
[41] A. G. Clark, K. Dierkes, and E. K. Paluch, Biophys. J. **105**, 570 (2013).
[42] E. Evans, R. Waugh, and L. Melnik, Biophys. J. **16**, 585 (1976).
[43] B. R. Brückner, A. Pietuch, S. Nehls, J. Rother, and A. Janshoff, Sci. Rep. **5**, 14700 (2015).
[44] E. Moeendarbary, L. Valon, M. Fritzsche, A. R. Harris, D. A. Moulding, A. J. Thrasher, E. Stride, L. Mahadevan, and G. T. Charras, Nat. Mater. **12**, 253 (2013).
[45] M. L. Gardel, F. Nakamura, J. Hartwig, J. C. Crocker, T. P. Stossel, and D. A. Weitz, Phys. Rev. Lett. **96**, 088102 (2006).
[46] N. Y. Yao, C. P. Broedersz, M. Depken, D. J. Becker, M. R. Pollak, F. C. MacKintosh, and D. A. Weitz, Phys. Rev. Lett. **110**, 018103 (2013).
[47] S. Sen, S. Subramanian, and D. E. Discher, Biophys. J. **89**, 3203 (2005).